Pushed to the edge: hundreds of myosin 10s pack into filopodia and could cause traffic jams on actin

Julia Shangguan[1], Ronald S. Rock[1,2*]

[1]Department of Biochemistry and Molecular Biology,
[2]Institute for Biophysical Dynamics,
The University of Chicago, Chicago, Illinois, USA

*To whom correspondence should be addressed: rrock@uchicago.edu

Abstract

Myosin 10 (Myo10) is a motor protein well known for its role in filopodia formation. Although Myo10-driven filopodial dynamics have been characterized, there is no information about the absolute number of Myo10 molecules during the filopodial lifecycle. To better understand molecular stoichiometries and packing restraints in filopodia, we measured Myo10 abundance in these structures. Here we combined SDS-PAGE densitometry with epifluorescence microscopy to quantitate HaloTag-labeled Myo10 in U2OS cells. About 6% of total intracellular Myo10 localizes to filopodia, where it is enriched at opposite ends of the cell. Hundreds of Myo10 are found in a typical filopodium, and their distribution across filopodia is log-normal. Some filopodial tips even contain more Myo10 than accessible binding sites on the actin filament bundle. Live-cell movies reveal a dense cluster of over a hundred Myo10 molecules that initiates filopodial elongation. Hundreds of Myo10 molecules continue to accumulate during filopodial growth, but that accumulation ceases when filopodia begin to retract. Rates of filopodial elongation, second-phase elongation, and retraction are inversely related to Myo10 quantities. Our estimates of Myo10 molecules in filopodia provide insight into the physics of packing Myo10, its cargo, and other filopodia-associated proteins in narrow membrane compartments. Our protocol provides a framework for future work analyzing Myo10 abundance and distribution upon perturbation.

Introduction

Myosins are a group of motor proteins that travel along the cell's dynamic cytoskeletal highways, binding actin and using ATP as fuel. Apart from myosin 2, the other >40 classes are considered 'unconventional' and often include membrane and cargo-binding tail domains[1]. A myosin of particular interest is myosin 10 (Myo10), a motor protein well known for its role in cellular protrusions[2,3]. These protrusions, termed filopodia, comprise tightly packed, parallel actin filaments and participate in a multitude of processes such as phagocytosis, directed cell migration, growth-cone guidance, and cell-cell adhesion[3]. Myo10 has key implications in health dysregulation[4]. For example, upregulated Myo10 is tied to increased genomic instability[5] and breast cancer aggressiveness[6].

Myo10's role in filopodia has been widely investigated[2,7–18]. Myo10 expression increases dorsal filopodia, and the cargo-binding tail domains, MyTH4 and FERM, are crucial for filopodia formation[9]. When Myo10 is overexpressed, it produces many Myo10 tip-localized filopodia[9,19,20]. Estimations on Myo10-positive filopodia length, average number of filopodia per area, and the velocities of extension and retraction have been reported[9,2,19,21,22]. However, questions regarding the quantity and distribution of Myo10 molecules within the cell still linger. Published images of Myo10 show its prominent localization in the filopodial tip, but a pool of Myo10 in the cell body remains[23,24]. A quantitative understanding of Myo10 localization could provide further insight into filopodial dynamics, how the crowded environment inside a thin filopodium affects the composition of the filopodial tip complex, and ultimately how Myo10 dysregulation connects to pathology.

Studies estimating protein numbers in subcellular compartments have been conducted before[25,26–28]. Methods include super-resolution microscopy[28], mass spectrometry[29,30], quantitative western blots[25], and photobleaching experiments[31]. We describe here a simple imaging and analysis method exploiting HaloTag labeling technology applied to Myo10 and filopodia. Similar to quantitative Western blotting of GFP[25], our strategy relies on SDS-PAGE densitometry using a fluorescent protein standard to estimate the mean number of Myo10 molecules per cell. In parallel fluorescence microscopy work, we record the fluorescent intensity per cell and convert the per-pixel fluorescent signal to the local number of molecules.

We find that the bulk of Myo10 remains in the cell body, with hundreds of Myo10s in each filopodium. Myo10 is unevenly distributed across a cell's filopodia, and some filopodial

tips have an excess of Myo10 over accessible actin filament binding-sites. Filopodial initiation from the membrane occurs from a median-sized cluster of 160 Myo10 molecules. Hundreds of Myo10 molecules continue to accumulate in filopodial puncta during filopodial extension phases, but accumulation ceases during filopodial retraction. Nascent filopodial extension, second-phase extension, and retraction rates all diminish with increasing Myo10 amounts, suggesting that a large number of motors suppress filopodial dynamics. Having the number of Myo10 molecules contextualizes interactions of Myo10 with its cargo, the plasma membrane and actin, building a picture of a densely-packed filopodial tip compartment.

Results

HaloTag-based cellular protein quantitation for microscopy

We expressed human HaloTag-Myo10 in U2OS cells to visualize its behavior in filopodia. Wildtype U2OS cells produce few filopodia, but exogenous expression of Myo10 induces abundant surface-attached filopodia (Fig. 1A). This induction suggests that Myo10 is a limiting reagent for filopodia in U2OS cells and allows us to assess the impact of variable Myo10 expression levels. HaloTag labeling was selected due to its high-efficiency binding and the commercial availability of a HaloTag standard protein with a known concentration. Our human, full-length Myo10 construct has an N-terminal HaloTag and C-terminal Flag-tag. Both N-terminal and C-terminal labeled Myo10 have nearly identical fluorescence staining patterns (Supplementary Fig. 1A).

To estimate the number of Myo10 molecules within specific cellular compartments, we combined SDS-PAGE and epifluorescence microscopy. First, we loaded lysate from a known number of Myo10-transfected U2OS cells on an SDS-PAGE gel along with known amounts of HaloTag standard protein, a 61 kDa HaloTag-GST fusion protein (Fig. 1B-C, Supplementary Fig. 1C). Because all samples were incubated with TMR-HaloTag ligand, we use the standard protein's fluorescence emission in the gel to generate a standard curve and estimate the mean number of Myo10 molecules per cell by densitometry. We propagate the 95% CI from the gel standard curve for our subsequent error estimates. In parallel, we measured TMR-HaloTag Myo10 molecules for the same set of transfected U2OS cells using epifluorescence microscopy. From these measurements, we obtain the total background-subtracted fluorescence intensity for each of the ~50-cell biological replicates (independent transfections on different days) per fixed

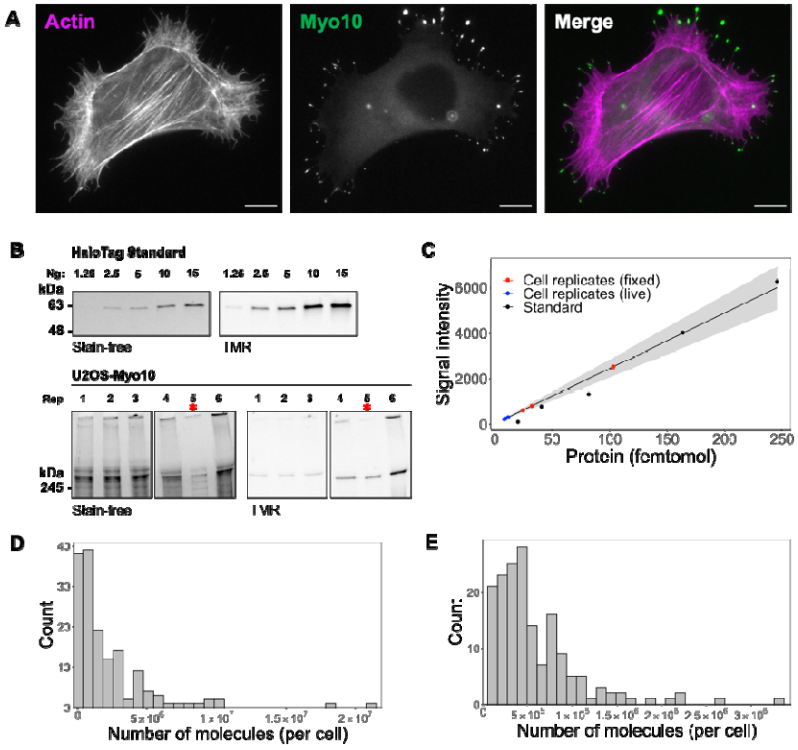

Fig. 1 | Hundreds of thousands of Myo10 monomer molecules found in Myo10-transfected U2OS cells. (**A**) Epifluorescence image of exogenously expressed HaloTag-Myo10 in U2OS cells. Actin is labeled with phalloidin-AF633 (magenta). Myo10 is labeled with HaloTag ligand-TMR (green). Scale bar = 10 µm. (**B**) The top SDS-PAGE lanes show the indicated quantity (in ng) of HaloTag standard protein. The bottom SDS-PAGE lanes from the same gel show 50,000 cells from 6 separate U2OS transient transfections (except bioreplicate 5, indicated by a red asterisk (*), has 10,000 cells). Bioreplicates 1, 2 and 3 are from live-cell analysis, while bioreplicates 4, 5 and 6 are from fixed-cell analysis. Stain-free shows total protein signal, while TMR shows only TMR-HaloTag-Myo10 signal. Signal was integrated for full-length Myo10 (at ~250 kDa) and any Myo10 aggregated in the wells at the top of the panels. (**C**) Standard curve for TMR fluorescence signal of HaloTag standard protein (black dots) compared to signal from HaloTag-Myo10 U2OS cells (red dots = fixed cell experiments, blue dots = live cell experiments). The linear fit is y = 24.32x, where the y-intercept is set to 0. R^2 = 0.98. Standard error of slope = 1.42. Grey shading indicates the 95% confidence interval. (**D**) Distribution of the number of Myo10 molecules per fixed cell (N = 150 cell images; min = 39,000, 95% CI: 33,000-46,000; median = 1,000,000, 95% CI: 870,000-1,200,000; max = 21,000,000, 95% CI: 18,000,000-25,000,000; bins = 30). (**E**) Distribution of the number of Myo10 molecules per live cell as determined by quantification of the first frame of N = 168 cell movies (min = 79,000, 95% CI: 67,000-92,000; median = 450,000, 95% CI: 370,000-520,000; max = 3,300,000, 95% CI: 2,800,000-3,800,000; bins = 30).

and live cell experiments. We used these totals to determine the fluorescence signal per molecule by microscopy. Both microscopy and gel samples were labeled with excess HaloTag ligand (Supplementary Fig. 2A, 2D-E) to ensure maximal labeling of Myo10 molecules with no detectable nonspecific labeling (Supplementary Fig. 1D-E). All Myo10 molecule measurements accounted for our measured 90% TMR-HaloLigand labeling efficiency (Supplementary Fig. 2B). Importantly, wildtype U2OS cells do not express detectable levels of Myo10 (Supplementary

Fig. 1E) and generate few filopodia. Therefore, essentially all Myo10 molecules carry the HaloTag label, and these molecules are responsible for inducing the filopodia that we observe. We pooled measurements from the three bioreplicates, resulting in the analysis of 150 cells of varying Myo10 expression levels in fixed cell experiments, and 168 cells in live-cell experiments (Fig. 1D-E).

Limited quantities of Myo10 in filopodia

We start with observations in fixed cells that report the distribution of Myo10 throughout U2OS cells. Exogenous expression of Myo10 results in 12–116 Myo10-positive filopodia per cell (median: 55; Fig. 2A, Supplementary Fig. 1B). Varying filopodia density likely reflects cells at different stages of migration or signaling[2,32]. Despite cells containing a median of 1,000,000 (95% CI: 870,000-1,200,000) total Myo10 molecules (Fig. 1D), only a small proportion of Myo10 localizes to filopodia (median: 5.4%; Fig. 2B). This small proportion of filopodial Myo10 is likely due to a limited Myo10 activation signal that is necessary to relieve autoinhibition and begin processive motility along the filopodial shaft.

What does a cell's total Myo10 filopodial signal indicate about filopodia formation? Higher Myo10 filopodial signal correlates with more filopodia, and ~100x more Myo10 appears to boost filopodia by 3x (Fig. 2C). Likewise, higher total intracellular Myo10 correlates with more filopodia (Fig. 2D), which supports our earlier hypothesis that Myo10 limits filopodial production in U2OS cells.

Spatial patterning of Myo10-decorated filopodia

Interactions with membrane-bound proteins, small cytosolic factors, and cortical actin networks might impact where Myo10 is localized. If these influences operate beyond the average separation between filopodia, we might see correlated spatial patterns where Myo10 is concentrated in sets of nearby filopodia and depleted from other sets. Indeed, Myo10 is not uniformly distributed, instead concentrating in cellular zones at opposite ends of the cell (Fig. 2E & F, Supplementary Fig. 3). Cells display periodic stretches of higher Myo10 density along the cell membrane, and some cells even contain membrane regions devoid of filopodia and Myo10 (Supplementary Fig. 3).

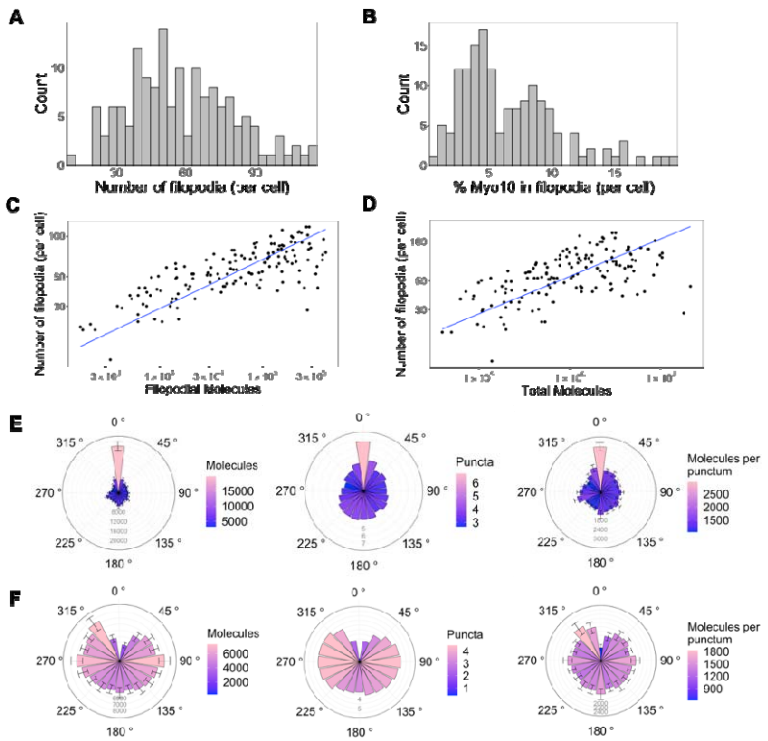

Fig. 2 | Only a small portion of intracellular Myo10 is activated and enters filopodia, and Myo10 is unevenly distributed around the cell. The following values are from fixed cell images. (**A**) Distribution of the number of Myo10-positive filopodia per cell (N = 8,733 Myo10-positive filopodia, 150 cells, min = 12, median = 55, max = 116). (**B**) Distribution of the percent of Myo10 localized in the filopodia per cell (N = 150 cells, min = 0.86%, median = 5.35%, max = 19.87%). (**C**) Correlation between number of Myo10-positive filopodia in a cell and the filopodial number of Myo10 molecules in the cell. The slope of power law function is 0.36. (**D**) Correlation between number of Myo10-positive filopodia in a cell and the total number of Myo10 molecules in the cell. The slope of power law function is 0.29. (**E**) Spatial correlation of Myo10-rich regions of the cell edge. Each cell was divided into 20 angular sections, and the section with the most molecules was aligned to 0°. Section quantities were then averaged across cells. Molecules, puncta, and molecules per punctum are shown. (**F**) Spatial correlation of Myo10-poor regions of the cell edge. As in E, but the section with the fewest molecules was aligned to 0° for each cell's rose plot. If >1 section contained no Myo10, a randomly selected empty Myo10 section was aligned to 0°. Error bars in E, F are the standard error of the mean for 500 bootstrapped samples of the 150 cells. Note the correlation of both molecules and puncta at opposite ends of cells (0°, 180°), and the anticorrelation with the two sides (90°, 270°).

Filopodia containing high Myo10 signal are surrounded by more neighboring filopodia, as evidenced by increased numbers of proximal Myo10 puncta (Fig. 2E, center). We define puncta as any cluster/spot of Myo10 detected by segmentation (see Methods for details on image segmentation analysis). The number of Myo10 per filopodium appears random and relatively fixed because the number of molecules per punctum is consistent (Fig. 2E, right). Potentially a local activation signal initiates filopodia at a particular site, and then the signal spreads from the high Myo10 zone to generate more puncta in the immediate vicinity. The opposite is weakly true, by which filopodia with low Myo10 levels tend to be next to fewer Myo10 puncta (Fig. 2F,

center). We noticed that a filopodial punctum can contain as few as ten Myo10 molecules (Supplementary Fig. 4A); these dim Myo10 puncta were primarily tip-localized (Supplementary Fig. 4B,C).

Myo10 often saturates accessible actin at filopodial tips

There is a vast range of Myo10 molecules per filopodium (median: 730 molecules, 95% CI: 610-850; Fig. 3A, B), and its distribution among filopodia is apparently log-normal (Supplementary Fig. 4D, E). Because log-normal distributions have long tails, we wondered how filopodia can support the movement of extreme Myo10 levels at filopodial tips. To address this question, we compared Myo10 concentrations to the amount of available actin sites in filopodia. We randomly selected a set of 90 filopodial tip-localized Myo10 puncta and measured the apparent length of the punctum. These lengths vary from ~250 nm (diffraction limited) to just over 1.5 µm in the case of the most elongated punctum. To estimate Myo10 concentrations, we used published values to define the geometry of a "typical" filopodium [33,34,35]. Considering a filopodium to be a cylindrical tube, we calculated local concentrations of Myo10 at filopodial tips using the number of molecules, the length of a Myo10 punctum, and a fixed radius of 100 nm[36]. At the tips, Myo10 ranges from ~ 6 µM to 560 µM (Fig. 3C, D).

Interestingly, Myo10 continues to flow into filopodia, even when there may be insufficient actin at the filopodial tip. To estimate the amount of F-actin available for binding, we modeled a filopodium of radius 100 nm comprising 30 actin filaments, of which 16 filaments are on the exposed surface of the bundle. Nagy *et al.* posited that only 4 of the 13 actin monomers per helical turn are available to Myo10 binding due to steric constraints within a fascin-actin bundle[34]. Using Zhuralev *et al.*'s equation[35] for calculating F-actin monomer concentration in a filopodium, we estimate that ~96 µM of actin monomers are available for Myo10 binding (see Supplementary Fig. 5 for full calculations).

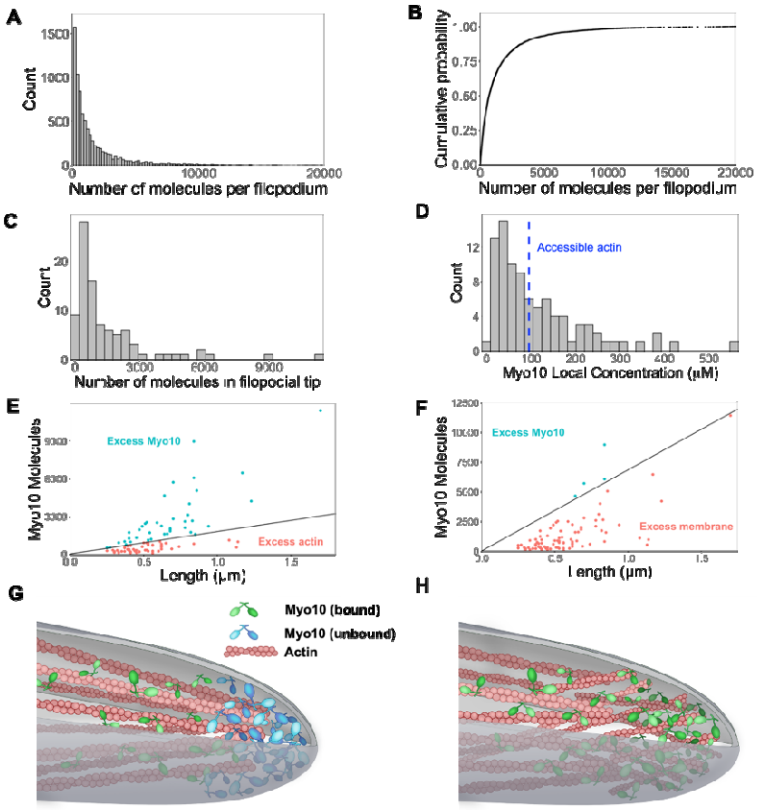

Fig. 3 | Hundreds of Myo10 molecules are found in a filopodium, potentially in excess over available actin at the filopodial tip. The following values are from fixed cell images. (**A**) Distribution of the number of Myo10 molecules per filopodium (N = 150 cells, 8,733 filopodia; min = 6, 95% CI: 5-7; median = 730, 95% CI: 610-850; max = 80,000, 95% CI: 67,000-93,000; 62 values >20,000 not shown; bins = 100). (**B**) Cumulative distribution function plot of data in part A. (**C**) Distribution of the number of Myo10 molecules at the filopodial tip (90 randomly chosen filopodia tip-localized Myo10 puncta from 9 different cell images; min = 66, 95% CI: 55-76; median = 788, 95% CI: 660-915; max =11,000, 95% CI: 9,600-13,000; bins = 30). (**D**) The local concentration of Myo10 at a filopodial tip. To estimate the volume, we measured the length of the filopodia tip-localized Myo10 puncta from part C in ImageJ. We then modeled filopodium as a cylinder of radius = 0.1 μm (published average). Min = 6.2 μM, 95% CI: 5.2-7.2; median = 84 μM, 95% CI: 70-97; max = 560 μM, 95% CI: 470-650, bins = 30. Blue dashed vertical line indicates the concentration of F-actin accessible for Myo10 binding in a filopodium (~96 μM). (**E**) Scatterplots of molecules vs. length for the puncta from part C. The phase boundary shows the 96 μM threshold from part D. (**F**) As in part E, but the line represents an estimate of allowable Myo10 on the filopodial tip membrane area. See supplementary Fig. 5 for membrane occupancy estimates. (**G**) Model of a Myo10 traffic jam at the filopodium tip. Not enough available actin monomers results in a population of free Myo10 (in blue). The free Myo10 is detached from actin but potentially still membrane-associated. (**H**) Model of frayed actin filaments at the filopodium tip. If actin filaments are not neatly packed into parallel bundles at the filopodium tip, disorganized and frayed actin filaments yield more accessible binding sites to Myo10.

If a filopodium contains ~96 μM of F-actin available to Myo10, and up to 560 μM Myo10, then sometimes Myo10 appears in excess (Fig. 3D, E). While excess Myo10 is not attached to actin, it may still be docked on the plasma membrane. In this scenario, we estimate available membrane area to include the curved hemisphere area and additional membrane space

occupied by the length of the Myo10 tip-localized puncta in Fig. 3C. We likewise estimate the footprint of the Myo10 C-terminal cargo binding domains, including those involved in membrane binding (see Supplementary Fig. 6 for details). We find that with even relatively large footprint estimates, there is still sufficient membrane area for filopodial tip-localized Myo10 (Fig. 3F). In the four cases where the available membrane is exceeded in Fig. 3F, it is likely because excess Myo10 causes a bulbous extension of the filopodial tip. This extension would provide more area for binding compared to a stereotypical, cylindrical filopodium, since a sphere enclosing a cylinder offers more surface area than a hemispherical cap.

This scenario of excess Myo10 at the filopodial tip would inevitably lead to a molecular traffic jam within the filopodia (Fig. 3G, Supplementary Fig. 5), during which Myo10 likely remains bound to the plasma membrane (Fig. 3F, Supplementary Fig. 6). Alternatively, the ends of actin bundles could be frayed at filopodial tips, increasing the available actin binding sites for Myo10 (Fig. 3H).

Myo10 accumulation over the filopodial lifecycle

All the above observations are based on fixed U2OS cells and therefore provide a static view of filopodial systems. To understand Myo10 levels and how they change during the dynamic filopodial lifecycle, we adapted our fluorescence calibration method for live cell imaging. We found it critical to rapidly collect 50–60 snapshots of individual cells for the calibration before collecting our movies on each sample. Adequate temperature control of the sample was also crucial, as the U2OS cells would rapidly contract their filopodia in response to cold. We identified and focused on three events in the filopodial lifecycle: filopodial initiation from a Myo10 punctum that appears at the plasma membrane, second-phase elongation from a Myo10 tip punctum in an established filopodium[19], and filopodial retraction.

Because Myo10 seems to be limiting filopodial production in U2OS cells, we wondered how many Myo10 molecules are needed for filopodial initiation. As Myo10 coalesces at a site on the plasma membrane and prepares to shoot into a filopodium, a median of 160 molecules gather in the punctum (Fig. 4A, Movie 1). The minimal value at the initiation site is 52 molecules, which may represent the lower limit of Myo10 needed for filopodial initiation. Although we attempted to observe Myo10 coalescence at the site of nascent filopodium, we were unable to detect them due to the limited sensitivity of the epifluorescence microscope. We did not use our

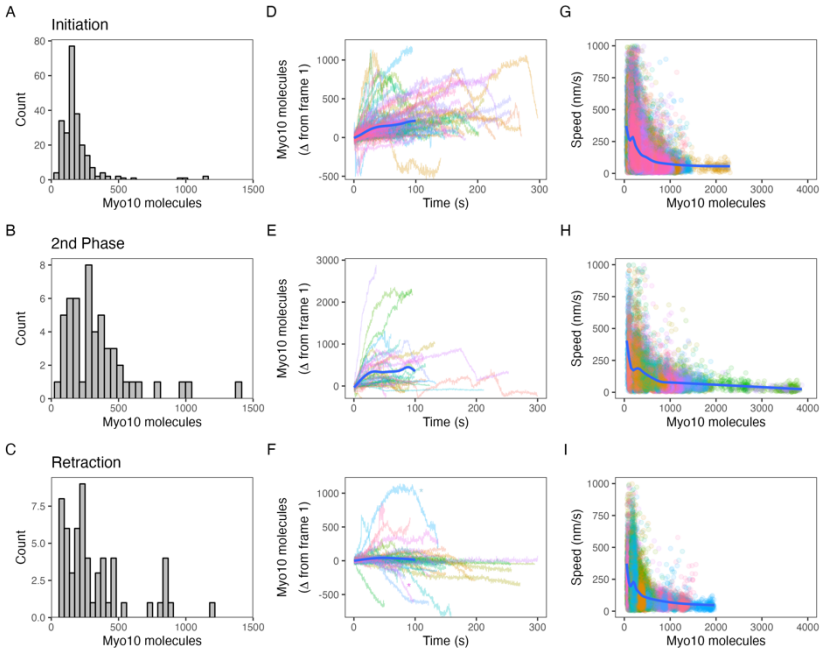

Fig. 4 | Myo10 dynamics from live cell movies. (**A-C**) Dense Myo10 puncta appear at the start of each phase of the filopodial lifecycle. Distributions of the number of Myo10 molecules in puncta upon: (**A**) Filopodial initiation (min = 52, 95% CI: 44-61; median = 160, 95% CI: 140-190; max = 1200, 95% CI: 970-1,300). (**B**) Second-phase elongation (min = 65, 95% CI: 54-75; median = 290, 95% CI: 240-340; max = 1,400, 95% CI: 1,200-1,600). (**C**) Filopodial retraction (min = 71, 95% CI: 60-82; median = 240, 95% CI: 200-280; max = 1,200, 95% CI: 1,000-1,400). Values are the means of the first two frames after spot detection and identification of filopodial lifecycle stage. Histograms A-C have 30 bins each. (**D-F**) Accumulation of Myo10 in puncta after filopodial initiation or second-phase elongation, but not after retraction. Evolution of number of molecules for each filopodial phase over time for: (**D**) Filopodial initiation. (**E**) Second-phase elongation. (**F**) Filopodial retraction. Starting values from (A-C) were subtracted from all traces to obtain delta over time. The generalized additive model (GAM) trend lines (blue) exclude long times (> 100 s) with few surviving trajectories. The outlier trajectory indicated by the magenta asterisk is from Movie 3, and the cyan asterisk is from Movie 4. (**G-I**) Myo10 punctum speeds are inversely correlated with the number of Myo10 molecules. Plots of instantaneous speeds vs. molecules for: (**G**) Filopodial initiation (min = 0.7, median = 160, max = 2,200 nm/s, Spearman's ρ = -0.51, $p < 2.2*10^{-16}$). (**H**) Second-phase elongation (min speed = 0.4, median = 110, max = 3,000 nm/s, Spearman's ρ = -0.55, $p < 2.2*10^{-16}$). (**I**) Filopodial retraction (min speed = 1.2, median = 140, max = 1,900 nm/s, Spearman's ρ = -0.45, $p < 2.2*10^{-16}$). Color signifies Myo10 puncta belonging to the same trajectory within each event type. Colors are independent in each panel. Blue lines are GAM trend lines. Panels A, D, G: 237 trajectories from 31 cells; B, E, H: 51 trajectories from 19 cells; C, F, I: 58 trajectories from 26 cells.

single-molecule TIRF microscopy because it has a limited field of view that is unable to capture an entire U2OS cell, which is needed to perform the fluorescence calibration.

Oftentimes, a new filopodial tip can emerge from an existing one in a process that we call second-phase elongation. Such a Myo10-induced multi-cycle filopodial elongation mechanism has been previously proposed[15]. We find a median of 290 Myo10 molecules organize and form the separate punctum at the start of second-phase elongation (Fig. 4B, Movie 2, Supplementary Fig. 7). This number represents about double the number of Myo10 involved in nascent

elongation (median: 160). Retracting Myo10 puncta initially contain a median of 240 molecules (Fig. 4C).

Both the initial punctum and the second-phase punctum accumulate additional Myo10 molecules over time (Fig. 4D, E). To estimate the accumulated amount, we took the last point of each trajectory and performed a t-test against the null hypothesis of a zero mean. Initial puncta accumulate a mean of 95 molecules (95% CI: 74, 120; t = 8.8; df = 236; p-value = $2.7*10^{-16}$), while second-phase puncta accumulate 307 molecules (95% CI: 130, 480; t = 3.5; df = 50; p-value = 0.001). However, unlike these two filopodial growth processes, retracting Myo10 puncta remain relatively constant as they return to the cell body (mean: -73 molecules; 95% CI: -140, -10; t = -2.3; df = 57; p-value = 0.025; Fig 4F). When retracting filopodia reach the cell body, the punctum often dissipates. However in a few cases, a new Myo10 punctum will coalesce and emerge from the location of a previous one (Movie 3).

Increasing quantities of Myo10 slow the punctum movements in all phases of the filopodial lifecycle

Finally, we wondered how the speeds of filopodial elongation and retraction are related to the number of Myo10 molecules in a tip punctum. Such values would help to constrain models that depend on Myo10 flux to deliver components to the filopodial tip or to generate force at the tip to assist actin polymerization. Interestingly, speeds of tip puncta during filopodial initiation, second-phase elongation, and retraction are all inversely related to the amount of Myo10 in the punctum (Fig. 4G-I). In each case, fewer molecules are associated with a higher variance in speed. The median speed of elongating Myo10 puncta is 160 nm/s, which is similar to previously published values[37,38,2,19]. Consistent with the trend of more molecules resulting in slower puncta velocities, the larger puncta involved in second-phase elongation display a slower median speed of 110 nm/s. The median speed of retracting Myo10 puncta is 110 nm/sec, similar to previously reported values[19]. For retracting puncta moving faster than actin retrograde flow, the velocity of Myo10 likely reflects a collapse of the whole filopodium or other complex filopodial dynamics. Our live movies capture some of these non-constant Myo10 retrograde events. Movie 4 exemplifies a decreasing intensity trajectory, wherein a Myo10 punctum rapidly ‘snaps’ closer to the cell body before diffusing into the cytoplasm. The ‘snap’ could be explained by the filopodium undergoing coiling or buckling, possibly induced in part by Myo10-generated force[39,40].

Discussion

Limited activation of Myo10

Myo10 is the limiting reagent for constructing filopodia in U2OS cells, but less than 20% arrives in filopodia when exogenously expressed (Fig. 2B). There is ample time for Myo10 to diffuse from the cytosolic pool to the numerous filopodial sites present in these cells, where it would then be captured. Thus, we expect that most of the cytosolic pool of Myo10 is in an inactive, autoinhibited state. Available PtdIns(3,4,5)P_3 (PIP_3) in the cell could be limiting the portion of free intracellular Myo10 that is activated and entering filopodia. Umeki *et al.* proposed that Myo10 binds PIP_3 at cell peripheries and dimerizes, becomes activated and converges local actin filaments to form the filopodial base[41]. Although Myo10 can participate in filopodia formation independently of VASP proteins and substrate attachment[9], other proteins have been found to be conserved in mechanisms of filopodia initiation. Components such as Cdc42[42], formin[43], Arp2/3 complex[44], neurofascin[32] or VASP[45,46] could also be prospective limiting partners of Myo10 entry into filopodia.

Prior information on the absolute number of Myo10 molecules in filopodia is sparse. Kerber *et al*. transfected HeLa cells with low levels of GFP-Myo10 (6-12 hours post-transfection) and found 20–200 molecules at the filopodial tip[38]. These levels are consistent with the range that we measure here (Fig. 3A). The shorter time post-transfection clearly affects Myo10 expression levels, which is evident in our data. Fixed cell experiments had higher Myo10 expression overall (48 hours post-transfection) compared to live cell experiments (24 hours post-transfection) (Fig. 1D, E).

Myo10 accretion into filopodial puncta

The distribution of Myo10 among filopodial puncta is log-normal rather than normal (Fig. 3A, B, Supplementary Fig. 4). This stands in contrast to more consistent, normally-distributed quantities of other actin-binding proteins. In fission yeast, proteins in the spindle pole body (e.g., Sad1p), at the cytokinetic contractile ring (e.g., Myo2p, Rho GEF Rgf1p), and within actin patches (e.g., ARPC1, capping protein Acp2p) did not display the wide concentration ranges that we saw for Myo10 in filopodia[25]. We propose several reasons for the non-Gaussian distribution of Myo10 molecules. Log-normal distributions are commonly associated with growth processes, and the accumulation of Myo10 at filopodial tips fits this description.

Filopodia have a large capacity for additional Myo10, and an ample reserve of unactivated Myo10 remains in the cytosol. Slow activation of Myo10 would then allow its travel down filopodia and accretion into puncta. Filopodia operate far from saturation, enabling relatively unrestricted Myo10 accumulation. In contrast, we suspect that the spindle pole body, cytokinetic ring, and actin patches represent cytoskeletal systems constructed from one or more limiting reagents. Limiting reagents put an upper bound on the growth of the system and lead to normal distributions at saturation.

Furthermore, the end requirements of cytokinesis and filopodial formation differ. Cytokinesis is a tightly regulated process involving a balance of forces, and the precise timing of each stage has been described in fission yeast[47]. Disruptions to components of the contractile ring, such as myosin inhibition, affect rates of actin filament disassembly and ring constriction[26]. In contrast, there is no specific number of filopodia that cells aim to create nor is there an optimal number of Myo10 per filopodium. Therefore, filopodia formation is a much more permissive process than cytokinesis, which could also explain the variation in values we observe of Myo10 compared to contractile ring-associated proteins.

Non-uniform Myo10 filopodial distribution

Myo10 tends to accumulate in filopodia that are at opposite ends of the cell (Fig. 2E, F). Thus, although Myo10 slowly accretes in individual filopodia, the accretion rate also varies spatially. We hypothesize a few different explanations for why Myo10 is not equally distributed around the cell. Potentially, Myo10 is funneled into filopodia that are moving towards specific environmental stimuli that simultaneously affect Myo10[48,49]. For example, local generation of PIP_3 might serve to dock and activate Myo10 in focused regions of the plasma membrane, such as the basolateral surfaces of polarized MDCK cells[50,23]. The docked Myo10 can then undergo 2D diffusion until it encounters the base of a filopodium. At the base, Myo10 switches to directed movement where it walks processively along the actin bundle to the tip. This overall diffusion and capture process for Myo10 has been observed at the single molecule level in cells, where it has been described as a 3D to 2D to 1D reduction in dimensionality[51].

Alternatively, Myo10 could be responding to information encoded in the actin network itself (e.g., nearby stress fibers) or other signaling molecules present in certain filopodia. Myosins can differentiate the structural and chemical properties of actin filaments, including age, tension, curvature, post-translational modifications, and multifilament architecture[52]. Thus, actin

filament networks could be partly responsible for choreographing Myo10 trajectories[52]. Future studies could identify potential guidance cues that Myo10-positive filopodia are responding to and identify other signaling proteins enriched in filopodia with high Myo10 signal.

An excess of Myo10 at the filopodial tip

A major finding of this work is that there is often an excess of Myo10 at filopodial tips over the available actin binding-sites for myosin (Fig. 3E-H). Interestingly, there is a mechanism that continues to push Myo10 into the filopodia, even when there may not be available actin to bind. This observation points to two notable features of motility in filopodial systems. The first is that there is no mechanism for a filopodium to shut off entry at the base when the tip is already overfilled with Myo10. The two sites are functionally independent of each other, although retracting filopodia differ in this regard (see below). The second is that Myo10 does not pack in an orderly fashion at the filopodial tip. Although our observations are in the context of an overexpression system, we note that immunofluorescence staining of endogenous Myo10 also shows occasional high-intensity, bulbous filopodial tips[20]. Our concentration estimates at the filopodial tip suggest that there is sufficient plasma membrane area for the Myo10. Therefore, even though Myo10 disengages from actin, it may remain engaged to the plasma membrane through its PH domains (Fig. 3F, Supplemental Fig. 6). As Myo10 molecules diffuse out of the concentrated region at the tip, they can encounter open sites on the actin filament bundle and reengage, walking back to the tip.

The structural model of the filopodium discussed above assumes an orderly, hexagonally close-packed bundle structure all the way to the filopodial tip. Consistent with this picture, EM images of mouse melanoma B16F1 cells indicate bundled parallel actin filaments at the filopodial tip[53]. However, this is not always the case. In *Dictyostelium discoideum* cells, actin filaments in the filopodia tip can terminate in free ends and/or appear fragmented, by which short actin filaments are arranged into a non-parallel array[54]. Bent filopodial tips in mammalian cells overexpressing GFP-Myo10 can display bulbous membrane extensions containing splayed actin filaments or actin filaments arranged in loops[55]. These fragmented, frayed, or otherwise disorganized ends of the filopodial actin bundle might support more actin-bound Myo10 (Fig. 3H). Indeed, an excess of Myo10 at the tip would compete with actin crosslinkers and help to support fraying. Further investigation is required to understand how Myo10 traffic jams and actin fraying affect the dynamics of actin itself and the activity of its associated proteins.

Number of Myo10 molecules needed for filopodial initiation and second-phase elongation

We observe a median of 160 Myo10 molecules and a minimum of 52 molecules at filopodial initiation (Fig. 4A). These quantities correspond to approximately 5 and 2 molecules per actin filament at a nascent filopodium, respectively. Watanabe *et al.* also saw a rapid (2-20 s) accumulation of Myo10 recruitment at filopodial initiation[19]. Myo10 participates in bridging actin filaments in emergent fascin-actin bundles, the actin structures that it prefers[3,37,56]. Such bridging could help to organize or orient the bundles to allow protrusion, much like the development of the lambda-precursors observed by Svitkina *et al*[53].

Second-phase filopodial elongation involves more molecules of Myo10, a median of 290 (Fig. 4B). This increase in number likely reflects the larger available pool of active Myo10 present at an established filopodial tip. Because only 160 molecules are needed for filopodial initiation, we believe that Myo10 quantities do not limit second-phase extension if initiation and second-phase elongation have similar mechanical requirements. Focal adhesion proteins, such as vinculin and integrin-β1, have been previously identified as essential components during the second-phase of filopodia extension[15]. Other actin-associated proteins (e.g., Arp2/3 and vinculin) are also present at this stage[15]. The duration required for focal adhesion proteins to translocate into a filopodium, coupled with actin crosslinking and bundling in the new filopodium, results in an increased accumulation of Myo10 at the local level. This accumulation is a consequence of Myo10 awaiting interaction with other protein partners at the filopodium tip. We speculate that the entire process takes longer than at the cell body plasma membrane, where the concentration of available focal adhesion proteins is higher.

Myo10 entry into filopodia switches off upon retraction

Myo10 accumulates within puncta after filopodial initiation and second-phase elongation (Fig. 4D, E), adding several hundred molecules on the minutes timescale. However, in retracting filopodia, accretion of additional Myo10 ceases (Fig. 4F). These retracting filopodia frequently have immediate neighbors that are not retracting. Therefore, the mechanism that switches off Myo10 traffic must be highly focused to single filopodia. Moreover, this switching mechanism must operate at the base of the filopodium where the Myo10 traffic would otherwise enter. Two mechanisms seem plausible given these considerations. Either the retracting filopodium generates a Myo10-inhibitory signal that diffuses out and rapidly dissipates, or the actin

architecture of the filopodium is altered and blocks Myo10 motility. These findings offer a quantitation of the dynamic behavior of Myo10 during retrograde flow, but further research is necessary to uncover the mechanisms governing switching of filopodial movement.

Multiple motors interfere to slow dynamic movements at the filopodial tip

The presence of increasing quantities of Myo10 slow filopodial movements in all three phases of the filopodial lifecycle (Fig. 4G-I). In reconstituted motility systems with multiple molecules, mechanically coupled motors typically move more slowly than uncoupled (or single) motors. This slowing is attributed to strain-sensitive motor coupling and motor dissociation limiting the collective velocity to some degree[57,58]. We propose that similar drag mechanisms operate here to slow the dynamics of filopodia.

Recent studies address the influence of filopodial-tip directed myosin motors on filopodial elongation. In work by Cirilo *et al.*, wildtype and fast-mutant Myo3 motors also localize to filopodial tips, and the filopodial elongation rate correlates with the Myo3 speed[21]. Myo3 is a slower motor than Myo10 (70 nm/s vs. 300-600 nm/s), and the Myo3-decorated filopodia move more slowly than we typically observe here[21]. These observations with slower myosins are consistent with our drag-based interference of filopodial dynamics: a coupled collection of slower motors would produce more drag than a collection of faster motors, all else being equal.

Limitations

Our experiments were conducted with the intention of minimizing biases and errors, but our results do come with caveats. Our results are within the context of an overexpression system, and other systems expressing endogenous Myo10 may express at a lower overall level than here. However, cells expressing endogenous Myo10 also show prominent dense tip-localization by immunofluorescence[20], so the Myo10 organization we see here does exist physiologically. Our goal in this study was to understand Myo10's role in filopodial initiation and dynamics in a defined system where Myo10 is the limiting factor. U2OS cells express undetectable levels of endogenous Myo10 (Supplementary Fig. 1E), so we are indeed observing the influence of Myo10 in a situation where Myo10 is the limiting factor for filopodia formation.

Regarding aspects of microscopy and automated image processing, very dim Myo10 spots could have escaped detection. During fixed and live imaging, we are unable to detect single molecules of Myo10 because we do not have the sensitivity of TIRF. Furthermore, our estimates of molecules are predicated on the calibration curve of the HaloTag standard protein on the SDS-PAGE gels, which is likely the highest source of error on our molecule counts. Despite these concerns, our values still provide a sense of the magnitude of Myo10 molecules within cellular structures.

Ideas & Speculation

One of our key findings is the excess of Myo10 compared to available actin at filopodial tips. We propose that there is a sizable population of Myo10 docked on the plasma membrane but not to actin (Figure. 4G). Alternatively, actin filaments that fray from the fascin-actin bundle yield more binding sites for Myo10 (Fig. 4H). Myo10 moves processively along actin bundles, even disorganized ones formed by crowding reagents[37]. Any single overloaded filopodium may use either or both mechanisms.

We argue that there is an interplay between incoming Myo10 that release upon encountering a traffic jam of other Myo10 molecules, and Myo10 molecules that are part of the traffic jam that are "pushed off" (i.e., naturally dissociate and are replaced) by new arrivals. Myo10 cargoes may need to handle either the actin-attached or actin-detached situation, which has implications for force-sensing cargoes such as integrins.

At the filopodial tip, we expect that newly formed actin will be rapidly occupied by Myo10 due to the high quantity on standby. However, fascin must eventually bind to facilitate the bundling of new actin. While Myo10 cannot bind to the interior of a fascin-actin bundle due to insufficient space, the converse is also true: fascin cannot bundle a fully Myo10-bound actin filament until the Myo10 dissociates. Once there is an opening, fascin can outcompete Myo10 due to the high avidity interaction between fascin and actin[59]. Therefore, the dynamic association/dissociation of Myo10 at the filopodial tip may be essential for the continued elongation of the filopodium.

Conclusion

Knowing the number of Myo10 molecules in a filopodium provides insight into molecular packing geometries in confined intracellular spaces. This study showcases the high

density of molecules that can be packed into tight cellular compartments, captures the number of Myo10 molecules needed for filopodial initiation, and finds that Myo10 entry into filopodia switches off upon filopodial retraction. Our results contribute to understandings of molecular stoichiometries in filopodia and Myo10 abundance in these structures. Our protocol also provides a framework for future studies examining the factors that tune Myo10 density and distribution.

Methods

Plasmids and constructs

Full-length human Myo10 sequence was constructed in a pTT5 vector backbone plasmid by Gibson assembly[60]. The construct includes an N-terminal Halotag (Promega; GenBank: JF920304.1), the full-length human Myo10 sequence (nucleotide sequence from GenBank: BC137168.1), and C-terminal Flag tag (GATTATAAAGATGATGATGATAAA). A complete DNA sequence of the insert is included in supplemental information.

Cell culture

U2OS cells were passaged every 2 days and used under passage number 10 after thawing. Cells were grown in Gibco 1x DMEM (ThermoFisher, 11995073) supplemented with 10% fetal bovine serum at 37 °C and 5% CO_2.

Transient transfection and coverslip seeding for fixed cell imaging

Cells were transiently transfected with 1 µg of the HaloTag-Myo10-FlagTag plasmid and 0.2 µg of a calmodulin plasmid using FuGENE HD Transfection reagent. Forty-eight hours after transfection, cells were detached using Accutase and seeded onto Ibidi 8-well chamber slides coated with 20 µg/ml laminin for imaging and onto 6 well dishes for SDS-PAGE analysis. After 3-4 hours, cells were collected for SDS-PAGE analysis at the same time as cells were fixed for microscopy. Three bioreplicates were conducted.

Transient transfection and coverslip seeding for live cell imaging

Cells were transiently transfected with 1 µg of the HaloTag-Myo10-FlagTag plasmid and 0.2 µg of a calmodulin plasmid using Lipofectamine 2000. Twenty-four hours after transfection, cells were seeded onto #1.5 coverglass bottom 35 mm petri dishes (Cellvis or MatTek) coated

with 20 µg/ml laminin for imaging and onto 6 well dishes for SDS-PAGE analysis. After 3-4 hours, cells were collected for SDS-PAGE analysis right before cells were live-imaged. Three bioreplicates were conducted.

Preparing cell lysates for SDS-PAGE

Cells growing in the 6 well plate were first incubated with Accutase for 15 min at room temperature. For live cell experiments, the Accutase additionally contained 0.75 µM TMR-HaloLigand. Accutase was neutralized with DMEM +10 % FBS and the cells were collected with a 3:30 min spin at 400 rcf at room temperature. The pellet was resuspended in 100 µl cell media, and 10 µl of the cells were removed and mixed with 1x Trypan blue for cell counting. The remaining cells were combined with 400 µl cell media and subjected to a 5 min, 400 rcf spin at room temperature. Cells were moved to ice post-spin and lysed in RIPA buffer containing 1 mM PMSF. Lysate samples were stored at -80 °C.

SDS gel analysis for Myo10 quantitation

HaloTag standard protein (Promega, G4491) samples, with 0.5 µM TMR-HaloLigand, were prepared for final masses of 1.25 ng, 2.5 ng, 5 ng, 10 ng and 15 ng and cell lysate samples (from live and fixed cell experiments) containing 50,000 cells on the gel. Excess TMR-HaloLigand was incubated for 10 min on ice with only lysates from the fixed cell experiments. All samples were supplemented with an SDS loading buffer (0.1 M DTT, 2% SDS, 0.05% bromophenol blue, 0.05M Tris-HCl, 10% glycerol, pH 6.8) and heated at 70°C for 10 min before loading onto a 4-20% Mini-PROTEAN TGX Stain-Free protein gel (BioRad, 4568095). The gel was run at 180 V for 45 min and imaged on a ChemiDoc. Images of the stain-free, AF647, and rhodamine channels were taken. We used the Gel Analysis plugin in ImageJ to compare signal intensity of the gel bands. A standard curve was generated from the HaloTag standard protein TMR signal to estimate the number of Myo10 molecules per total transfected cells loaded (total cells loaded times the fraction transfected). Microscopy was used to count the percentage of transfected cells from ~105-190 randomly surveyed cells per bioreplicate.

Western blotting for Myo10 in U2OS cells

We loaded 50,000 cells of wild-type and Myo10-transfected U2OS cells for SDS gel analysis as described earlier. The gel was transferred to PVDF membrane using a Pierce Power Blotter semi-dry electrophoretic transfer cell (1.3 A constant for 12 min). The blot was blocked

with 5% milk in 1x TBST, 1 hour shaking at room temperature. For 1 hour at room temperature, the blot was incubated with anti-Myosin10 (Novus NBP1-87748) and anti-β-tubulin (Invitrogen 22833) antibodies in 5% milk in 1x TBST. The blot was rinsed with 5% milk in 1x TBST for 10 min, three total washes. Then, the blot was incubated with anti-Rabbit-HRP (Cell Signaling 7074) and anti-Mouse-HRP (Cell Signaling 7076) antibodies in 1x TBST, 1 hour shaking at room temperature. After three 10 min washes with 1x TBST, chemiluminescent substrate (Thermo Scientific, SuperSignal West Femto, 34094) was applied to the blot for 2 min and subsequently imaged on a Chemidoc.

TMR-HaloLigand labeling efficiency

To test TMR-HaloLigand labeling efficiency, 6.8 µM of HaloTag standard protein was labeled with TMR-HaloLigand in 5.8x molar excess in a 20 µl reaction volume, on ice for 10 min. Bio-Beads SM-2 (BioRad, 152-8920) were washed with methanol 3x, distilled water 3x, and PBS 3x before they were added to ¼ volume of the reaction. After 1 hour and 40 min at RT in the dark, the reaction tube was spun for 3 min, 600 rcf spin. The supernatant was recovered and the absorbance spectrum was measured on Nanodrop. Absorbances at 280 nm and 553 nm were used for protein and dye concentrations, respectively. To account for protein that may have nonspecifically bound to the beads, pre-bead TMR-HaloLigand-labeled HaloTag standard protein was loaded on an SDS-PAGE gel alongside the post-bead supernatant. Comparing the signal intensities of pre- and post-bead gel bands allowed for a corrected post-beads protein concentration value.

Ligand labeling saturation for microscopy

To test ligand labeling saturation for microscopy, cells were fixed for 20 min in a solution comprising: 4% PFA, 0.08% Triton, 1:1000 DAPI in PEM buffer and a series of TMR-HaloLigand concentrations (in µM: 0.05, 0.1, 0.5, 1, 2.5, 5). Live cells were incubated with DMEM +10 % FBS containing TMR-HaloLigand (in µM: 0.05, 0.1, 0.5, 0.75, 1, 2.5 µM) at 37°C, 5% CO_2 in the dark. After 10 min, cells were washed and incubated with GOC during live imaging as described earlier.

Image analysis was done using in-house Python scripts. Images were background subtracted using a rolling ball radius of 50 pixels in ImageJ. To obtain total intracellular Myo10 signal in fixed cells, the phalloidin stain was used as a guide to manually draw bound cells.

Filopodial puncta, segmented by watershed segmentation, were used to generate a convex hull mask. Signal inside the mask was summed.

To obtain total intracellular Myo10 signal in live cells, filopodial puncta, segmented by watershed segmentation, were used to generate a convex hull mask. Signal inside the convex hull mask was summed. Because there was higher, uneven background that persisted after the rolling ball subtraction in higher TMR-HaloLigand live samples, segmented Myo10 puncta were summed and plotted as well. Plotting only segmented puncta appeared to reduce the contribution of background pixels inside the convex hull mask that could falsely inflate final Myo10 intracellular signal.

Fixed-cell fluorescence microscopy

For Myo10 fixed cell imaging, cells were fixed for 20 min in a solution comprising: 4% PFA, 0.08% Triton, 2.5 µM TMR-HaloLigand, and 1:1000 DAPI in PEM buffer. After 3 PBS washes (4 min each), cells were stained with 1 mM Phalloidin-AF633 in 1% BSA for 20 min. Cells were washed 3x with PBS (4 min each) before immediate imaging. Fluorescence images were taken on an Axiovert using a 60x water objective and a gain of 125 and 175 ms exposure (below detector saturation). To prevent photobleaching, cells were kept in the dark and imaged immediately upon illumination of the selected field of view. Samples were imaged within a day of preparation. TMR was visualized using green light and AF633 was visualized with red light.

Analyzing fixed cell images

Image analysis was done using in-house Python scripts. To calculate the number of Myo10 molecules in the fluorescence images, the Myo10-stained images were first background subtracted: the average signal of a 56 x 56 pixel square near the cell body was calculated and subtracted from each pixel of the TIFF image. Next, the phalloidin-stained cell image and Myo10-stained image were filtered to remove non-cell objects and subjected to watershed segmentation. To generate a ‘cell body mask’, an erosion function followed by an opening function were applied to the phalloidin-stained cell image. The Myo10 image mask was defined as the ‘total cell mask.’ The ‘cell body mask’ was subtracted from the ‘total cell mask’ for a ‘filopodia mask.’ Connected component analysis (CCA) was performed on the ‘filopodia mask’ to obtain masks for all filopodia-localized Myo10 puncta. For the CCA, pixels were considered neighbors if they were connected through a maximum of 2 orthogonal hops. Segmented puncta

(i.e. the connected regions) were then inspected in Napari[61]. Puncta belonging to the same filopodium were manually combined into the same filopodium mask. Signal in each filopodium mask and within the 'cell body mask' were summed. For each bioreplicate, a 'total pool' of Myo10 molecules was calculated by multiplying the average Myo10 molecules per transfected cell (as determined from the SDS-PAGE gel) by the number of cell images analyzed. Within each bioreplicate, the signal intensities were summed for all cells. Therefore, to get the number of molecules within a Myo10 filopodium, the filopodium intensity was divided by the bioreplicate signal intensity sum and multiplied by 'total pool.' To calculate percentage of Myo10-positive filopodia, total filopodia per cell were manually counted.

Measuring Myo10 orientation distribution in fixed cell filopodia

To generate the rose plots of the Myo10 distribution in filopodia, each cell was divided into 20 radial sections from the cell's center of mass. The Myo10 filopodial molecules were averaged within each section. The section with the highest molecules was aligned to degree 0 for each cell's rose plot. Total count of Myo10 puncta analyzed per section was also calculated. Puncta were not manually combined if belonging to the same filopodium. Therefore, puncta that were at the border of two radial sections were counted once for each section. For the rose plots in panel 2D, a randomly selected empty Myo10 section was aligned to degree 0 if more than one section contained no Myo10. The standard error bars represent the standard error of the mean molecules per section after 500 iterations of bootstrapping. In each iteration, 150 cells were randomly selected with replacement.

Measuring local Myo10 concentrations at the tips of fixed cell filopodia

To obtain estimates of local Myo10 concentrations in filopodia tips, 10 Myo10 tip-localized puncta were randomly chosen from 3 different cell images of each bioreplicate set. The length of each punctum was measured in ImageJ. The volume occupied by the Myo10 punctum was estimated using the volume of a cylinder: length = height and width = 2*radius, where radius was assumed to be 100 nm (reported average radius) because of the resolution limit. The signal intensity of the Myo10 punctum was converted to molecules as described above.

Available actin monomer concentration for Myo10 binding is described in Supplementary Figure 5. Available membrane surface for Myo10 binding is described in Supplementary Figure 6.

Staining cells for live cell imaging

For Myo10 live imaging, cells were incubated with DMEM +10 % FBS containing 0.75 µM TMR-HaloLigand at 37 °C in the dark. After 10 min, cells were quickly washed 2x with DMEM +10 % FBS washes, and one 5 min wash. Immediately before imaging, cells were replaced with DMEM +10 % FBS containing 1x GOC. Live cells were imaged on a 37 °C heated objective using a gain of 100 and 300 ms exposure (below detector saturation). Ten random cells per bioreplicate were recorded for <6 minutes (three bioreplicates in total). For each bioreplicate, additional snapshots of ~50 living cells were taken to sample the intensity distribution for the fluorescence intensity-to-molecule conversions. Fixed cell samples were prepared in parallel to obtain transfection efficiencies of the bioreplicates.

Analyzing live cell movies

Image analysis was partially done using in-house Python scripts. To get an intensity distribution for the fluorescence intensity-to-molecule conversions, the Myo10-stain snapshots were first background subtracted using a rolling ball radius of 50 pixels in ImageJ. To obtain total intracellular Myo10 signal, filopodial puncta were used as bounding edges for a manually drawn mask. Signal inside the drawn mask was summed. For each bioreplicate, a 'total pool' of Myo10 molecules was calculated by multiplying the average Myo10 molecules per transfected cell by the number of cell images analyzed. Within each bioreplicate, the signal intensities were summed for all cells. Therefore, to get the number of molecules within a Myo10 punctum, the punctum intensity was divided by the bioreplicate signal intensity sum and multiplied by the 'total pool.' Myo10 puncta in the live cell movies were segmented and tracked using the Fiji plugin TrackMate[62]. Trackmate parameters used: LoG detector with estimated blob diameter = 1 µm, median filter, sub-pixel localization; LAP tracker with frame to frame linking = 0.5 µm, track segment gap closing = 1 µm (max frame gap=2), track segment splitting = 0.5 µm, track segment merging = 1 µm.

After completing TrackMate analysis, all trajectories in the cell movies were manually inspected for occurrence of three types of filopodial events. The start of the three events are

defined by when TrackMate first segments the punctum. “Initiation” is when a Myo10 punctum gathers at the plasma membrane and then shoots into a filopodium. “Second-phase elongation” is a new Myo10 punctum that emerges from an existing one. “Retraction” is when a Myo10 punctum, observed in frame 1 of the movie, begins moving back towards the cell body. The track IDs were recorded for each trajectory type and further inspected. A few puncta that TrackMate segmented were manually removed because they were clearly background noise or incorrectly tracked puncta (*e.g.*, a punctum from another filopodium that briefly crosses paths, or filopodial puncta that were detected by TrackMate only well after initiation). Any selected trajectories containing Myo10 puncta merging or splitting events were excluded from velocity analysis.

For Figure 4 parts A-C, Myo10 puncta molecules in the first two frames of each trajectory were averaged. For Figure 4 parts D-F, the starting punctum molecules are subtracted from subsequent frames of each trajectory. Parts D-E follow the trajectory of each punctum that is initially identified for a certain filopodial event, but then those puncta could have engaged in other activities during their lifetime (e.g. retract). GAM fitting was only applied to a subset of the total data to prevent a few long trajectories from dominating the trend. For Figure 4 parts G-H, velocity analysis does not only account for Myo10 punctum that moved away from the starting point of the trajectory. For Figure 4 parts G-I, puncta merging or splitting events were excluded from analysis.

Supplemental Material

Movie 1 | Myo10 punctum initiates a nascent filopodium. Example of a Myo10 punctum (red circle) right as the filopodium shoots from the cell body. 300 ms exposure, 10 fps.

Movie 2 | Myo10 punctum can undergo a second elongation. Example of a Myo10 punctum (red circle) right after emergence from an existing filopodium. 300 ms exposure, 10 fps.

Movie 3. | Example of Myo10 punctum decreasing in intensity as it returns to cell body. The trajectory indicated by the blue asterisk in Figure 3E. Example of a Myo10 punctum (purple circle) that decreases in intensity before becoming the site of new filopodium growth. 300 ms exposure, 30 fps.

Movie 4. | Example of Myo10 punctum in a 'snapping' filopodium as it returns to cell body. The trajectory indicated by the magenta asterisk in Figure 3E. Example of a Myo10 punctum (purple circle) that 'snaps' towards the cell body and then diffuses into the cytoplasm. 300 ms exposure, 30 fps.

Acknowledgments

We thank Eugene Schauchuk for designing and cloning the Myo10 construct, and Prof. David Kovar, Department of Molecular Genetics and Cell Biology, University of Chicago, for critical comments on the manuscript. This work was supported by the University of Chicago MCB Training Grant (T32 GM144292) and the NSF Graduate Research Fellowship (2140001) (to J.S.) and NIH grants R01GM124272 and R01GM149073 (to R.S.R.).

References Cited

1. Odronitz, F. & Kollmar, M. Drawing the tree of eukaryotic life based on the analysis of 2,269 manually annotated myosins from 328 species. *Genome Biol* **8**, R196 (2007).
2. Kerber, M. L. & Cheney, R. E. Myosin-X: a MyTH-FERM myosin at the tips of filopodia. *Journal of Cell Science* **124**, 3733–3741 (2011).
3. Mattila, P. K. & Lappalainen, P. Filopodia: molecular architecture and cellular functions. *Nat Rev Mol Cell Biol* **9**, 446–454 (2008).
4. Courson, D. S. & Cheney, R. E. Myosin-X and disease. *Experimental Cell Research* **334**, 10–15 (2015).

5. Mayca Pozo, F. *et al.* MYO10 drives genomic instability and inflammation in cancer. *Sci. Adv.* **7**, eabg6908 (2021).
6. Cao, R. *et al.* Elevated expression of myosin X in tumours contributes to breast cancer aggressiveness and metastasis. *Br J Cancer* **111**, 539–550 (2014).
7. Zhang, H. *et al.* Myosin-X provides a motor-based link between integrins and the cytoskeleton. *Nat Cell Biol* **6**, 523–531 (2004).
8. Tokuo, H. & Ikebe, M. Myosin X transports Mena/VASP to the tip of filopodia. *Biochemical and Biophysical Research Communications* **319**, 214–220 (2004).
9. Bohil, A. B., Robertson, B. W. & Cheney, R. E. Myosin-X is a molecular motor that functions in filopodia formation. *Proceedings of the National Academy of Sciences* **103**, 12411–12416 (2006).
10. Tokuo, H., Mabuchi, K. & Ikebe, M. The motor activity of myosin-X promotes actin fiber convergence at the cell periphery to initiate filopodia formation. *Journal of Cell Biology* **179**, 229–238 (2007).
11. Zhu, X.-J. *et al.* Myosin X regulates netrin receptors and functions in axonal path-finding. *Nat Cell Biol* **9**, 184–192 (2007).
12. Raines, A. N., Nagdas, S., Kerber, M. L. & Cheney, R. E. Headless Myo10 Is a Negative Regulator of Full-length Myo10 and Inhibits Axon Outgrowth in Cortical Neurons. *Journal of Biological Chemistry* **287**, 24873–24883 (2012).
13. Arjonen, A. *et al.* Mutant p53–associated myosin-X upregulation promotes breast cancer invasion and metastasis. *J. Clin. Invest.* **124**, 1069–1082 (2014).
14. Courson, D. S. & Cheney, R. E. Myosin-X and disease. *Experimental Cell Research* **334**, 10–15 (2015).

15. He, K., Sakai, T., Tsukasaki, Y., Watanabe, T. M. & Ikebe, M. Myosin X is recruited to nascent focal adhesions at the leading edge and induces multi-cycle filopodial elongation. *Sci Rep* **7**, 13685 (2017).
16. Heimsath, E. G., Yim, Y.-I., Mustapha, M., Hammer, J. A. & Cheney, R. E. Myosin-X knockout is semi-lethal and demonstrates that myosin-X functions in neural tube closure, pigmentation, hyaloid vasculature regression, and filopodia formation. *Sci Rep* **7**, 17354 (2017).
17. Summerbell, E. R. *et al.* Epigenetically heterogeneous tumor cells direct collective invasion through filopodia-driven fibronectin micropatterning. *Sci. Adv.* **6**, eaaz6197 (2020).
18. Miihkinen, M. *et al.* Myosin-X and talin modulate integrin activity at filopodia tips. *Cell Reports* **36**, 109716 (2021).
19. Watanabe, T. M., Tokuo, H., Gonda, K., Higuchi, H. & Ikebe, M. Myosin-X Induces Filopodia by Multiple Elongation Mechanism. *Journal of Biological Chemistry* **285**, 19605–19614 (2010).
20. Berg, J. S. & Cheney, R. E. Myosin-X is an unconventional myosin that undergoes intrafilopodial motility. *Nat Cell Biol* **4**, 246–250 (2002).
21. Cirilo, J. A., Liao, X., Perrin, B. J. & Yengo, C. M. The dynamics of actin protrusions can be controlled by tip-localized myosin motors. *Journal of Biological Chemistry* **300**, 105516 (2024).
22. Petersen, K. J. *et al.* MyTH4-FERM myosins have an ancient and conserved role in filopod formation. *Proc. Natl. Acad. Sci. U.S.A.* **113**, (2016).
23. Liu, K. C., Jacobs, D. T., Dunn, B. D., Fanning, A. S. & Cheney, R. E. Myosin-X functions in polarized epithelial cells. *MBoC* **23**, 1675–1687 (2012).

24. Kenchappa, R. S. *et al*. Myosin 10 Regulates Invasion, Mitosis, and Metabolic Signaling in Glioblastoma. *iScience* **23**, 101802 (2020).

25. Wu, J.-Q. & Pollard, T. D. Counting Cytokinesis Proteins Globally and Locally in Fission Yeast. *Science* **310**, 310–314 (2005).

26. Malla, M., Pollard, T. D. & Chen, Q. Counting actin in contractile rings reveals novel contributions of cofilin and type II myosins to fission yeast cytokinesis. *MBoC* **33**, ar51 (2022).

27. Loiodice, I. *et al.* Quantifying Tubulin Concentration and Microtubule Number Throughout the Fission Yeast Cell Cycle. *Biomolecules* **9**, 86 (2019).

28. Sayyad, W. A. & Pollard, T. D. The number of cytokinesis nodes in mitotic fission yeast scales with cell size. *eLife* **11**, e76249 (2022).

29. Zhang, G. *et al.* Protein Quantitation Using Mass Spectrometry. in *Computational Biology* (ed. Fenyö, D.) vol. 673 211–222 (Humana Press, Totowa, NJ, 2010).

30. Shin, J.-B. *et al.* Molecular architecture of the chick vestibular hair bundle. *Nat Neurosci* **16**, 365–374 (2013).

31. Hummert, J. *et al.* Photobleaching step analysis for robust determination of protein complex stoichiometries. *MBoC* **32**, ar35 (2021).

32. Peuhu, E. *et al.* MYO10-filopodia support basement membranes at pre-invasive tumor boundaries. *Developmental Cell* **57**, 2350-2364.e7 (2022).

33. Aramaki, S., Mayanagi, K., Jin, M., Aoyama, K. & Yasunaga, T. Filopodia formation by crosslinking of F-actin with fascin in two different binding manners: Bundling Mechanisms of F-Actin by Fascin in Filopodia. *Cytoskeleton* **73**, 365–374 (2016).

34. Nagy, S. & Rock, R. S. Structured Post-IQ Domain Governs Selectivity of Myosin X for Fascin-Actin Bundles. *Journal of Biological Chemistry* **285**, 26608–26617 (2010).

35. Zhuravlev, P. I., Lan, Y., Minakova, M. S. & Papoian, G. A. Theory of active transport in filopodia and stereocilia. *Proc. Natl. Acad. Sci. U.S.A.* **109**, 10849–10854 (2012).

36. Mogilner, A. & Rubinstein, B. The Physics of Filopodial Protrusion. *Biophysical Journal* **89**, 782–795 (2005).

37. Nagy, S. *et al.* A myosin motor that selects bundled actin for motility. *Proc. Natl. Acad. Sci. U.S.A.* **105**, 9616–9620 (2008).

38. Kerber, M. L. *et al.* A Novel Form of Motility in Filopodia Revealed by Imaging Myosin-X at the Single-Molecule Level. *Current Biology* **19**, 967–973 (2009).

39. Leijnse, N. *et al.* Filopodia rotate and coil by actively generating twist in their actin shaft. *Nat Commun* **13**, 1636 (2022).

40. Leijnse, N., Oddershede, L. B. & Bendix, P. M. Helical buckling of actin inside filopodia generates traction. *Proc. Natl. Acad. Sci. U.S.A.* **112**, 136–141 (2015).

41. Umeki, N. *et al.* Phospholipid-dependent regulation of the motor activity of myosin X. *Nat Struct Mol Biol* **18**, 783–788 (2011).

42. Krugmann, S. *et al.* Cdc42 induces filopodia by promoting the formation of an IRSp53:Mena complex. *Current Biology* **11**, 1645–1655 (2001).

43. Alieva, N. O. *et al.* Myosin IIA and formin dependent mechanosensitivity of filopodia adhesion. *Nat Commun* **10**, 3593 (2019).

44. Korobova, F. & Svitkina, T. Arp2/3 Complex Is Important for Filopodia Formation, Growth Cone Motility, and Neuritogenesis in Neuronal Cells. *MBoC* **19**, 1561–1574 (2008).

45. Lebrand, C. *et al.* Critical Role of Ena/VASP Proteins for Filopodia Formation in Neurons and in Function Downstream of Netrin-1. *Neuron* **42**, 37–49 (2004).

46. Arthur, A. L., Crawford, A., Houdusse, A. & Titus, M. A. VASP-mediated actin dynamics activate and recruit a filopodia myosin. *eLife* **10**, e68082 (2021).

47. Wu, J.-Q., Kuhn, J. R., Kovar, D. R. & Pollard, T. D. Spatial and Temporal Pathway for Assembly and Constriction of the Contractile Ring in Fission Yeast Cytokinesis. *Developmental Cell* **5**, 723–734 (2003).

48. Meyen, D. *et al.* Dynamic filopodia are required for chemokine-dependent intracellular polarization during guided cell migration in vivo. *eLife* **4**, e05279 (2015).

49. Efremov, A. K. *et al.* Application of piconewton forces to individual filopodia reveals mechanosensory role of L-type Ca2+ channels. *Biomaterials* **284**, 121477 (2022).

50. Lu, Q., Yu, J., Yan, J., Wei, Z. & Zhang, M. Structural basis of the myosin X $PH1_N$-PH2-$PH1_C$ tandem as a specific and acute cellular $PI(3,4,5)P_3$ sensor. *MBoC* **22**, 4268–4278 (2011).

51. Baboolal, T. G., Mashanov, G. I., Nenasheva, T. A., Peckham, M. & Molloy, J. E. A Combination of Diffusion and Active Translocation Localizes Myosin 10 to the Filopodial Tip. *Journal of Biological Chemistry* **291**, 22373–22385 (2016).

52. Santos, A., Shauchuk, Y., Cichoń, U., Vavra, K. C. & Rock, R. S. How Actin Tracks Affect Myosin Motors. in *Myosins* (ed. Coluccio, L. M.) vol. 1239 183–197 (Springer International Publishing, Cham, 2020).

53. Svitkina, T. M. *et al.* Mechanism of filopodia initiation by reorganization of a dendritic network. *The Journal of Cell Biology* **160**, 409–421 (2003).

54. Medalia, O. *et al.* Organization of Actin Networks in Intact Filopodia. *Current Biology* **17**, 79–84 (2007).

55. Li, W. *et al*. Chiral growth of adherent filopodia. *Biophysical Journal* **122**, 3704–3721 (2023).

56. Ropars, V. *et al.* The myosin X motor is optimized for movement on actin bundles. *Nat Commun* **7**, 12456 (2016).

57. Lu, H. *et al*. Collective Dynamics of Elastically Coupled Myosin V Motors. *Journal of Biological Chemistry* **287**, 27753–27761 (2012).

58. Hariadi, R. F., Cale, M. & Sivaramakrishnan, S. Myosin lever arm directs collective motion on cellular actin network. *Proc. Natl. Acad. Sci. U.S.A.* **111**, 4091–4096 (2014).

59. Courson, D. S. & Rock, R. S. Actin Cross-link Assembly and Disassembly Mechanics for α-Actinin and Fascin. *Journal of Biological Chemistry* **285**, 26350–26357 (2010).

60. Gibson, D. G. *et al*. Enzymatic assembly of DNA molecules up to several hundred kilobases. *Nat Methods* **6**, 343–345 (2009).

61. Sofroniew, Nicholas *et al.* napari: a multi-dimensional image viewer for Python. Zenodo https://doi.org/10.5281/ZENODO.3555620 (2022).

62. Tinevez, J.-Y. *et al.* TrackMate: An open and extensible platform for single-particle tracking. *Methods* **115**, 80–90 (2017).